Surface & Coatings Technology 209 (2012) 110–116

Contents lists available at SciVerse ScienceDirect

Surface & Coatings Technology

journal homepage: www.elsevier.com/locate/surfcoat

A thick TiN/TiCN multilayer film by DC magnetron sputtering

Jianyun Zheng [a,b], Junying Hao [a,*], Xiaoqiang Liu [a,b], Qiuyu Gong [a,b], Weimin Liu [a]

[a] State Key Laboratory of Solid Lubrication, Lanzhou Institute of Chemical Physics, Chinese Academy of Sciences, Lanzhou 730000, PR China
[b] Graduate University of Chinese Academy of Sciences, Beijing 100049, PR China

ARTICLE INFO

Article history:
Received 29 May 2012
Accepted in revised form 18 August 2012
Available online 27 August 2012

Keywords:
TiN/TiCN multilayer
Thick film
Microstructure and properties
Friction and wear

ABSTRACT

A thick TiN/TiCN multilayer film was prepared on steel and silicon (Si) substrates using a DC magnetron sputtering technique under a high deposition rate. Its thickness reached about 23.5 μm and it was composed of 30 bilayer numbers. X-ray photoelectron spectroscopy (XPS), X-ray diffraction (XRD), cross-sectional high resolution transmission electron microscopy (HRTEM) and field emitted scanning electron microscopy (FESEM) were employed to characterize the composition and structure of the film on the Si substrates. It was found that the inner TiCN layers consisted of a mixture nanocrystalline TiCN phase and amorphous carbon, and the TiN layers showed nano-columnar structure. The adhesion force and the hardness of the film deposited on steel substrates were 29.0 N and 21.4 GPa, respectively. It was revealed that the thick film still maintained the excellent mechanical properties. The film sliding against steel ball had good wear resistance and very long service life (>11 h) in ambient air under high rotate speed and large load.

1. Introduction

Currently, to prevent severe wear, a series of titanium carbonitride (TiCN)-based films are deposited by applying different physical vapor deposition (PVD) techniques. Recently, the new generation TiCN-based films such as multicomponent (TiAlCN, TiNOC) [1,2], multilayer (TiN/TiCN/TiC) [3], graded (Ti/TiN/TiCN) [4] and composite [5,6] films have drawn the attention of researchers. They think that the properties of these new TiCN-based films are better than that of the traditional TiCN films. The TiN/TiCN multilayer films have shown good chemical stability, superior mechanical properties, and excellent wear and corrosion resistance. In the work by Su and Kao [7], it was found that the 7 μm-thick TiN/TiCN/TiN multilayer films containing a double-layer TiN (2 μm) and TiCN (2 μm) with a top layer of TiN (3 μm) had a good wear resistance, but around 9 μm-thick films performed a bad wear resistance due to the poor adhesion. In addition, Raveh et al. [8] have reported that the 3 μm-thick TiN/TiCN films (0.8 μm TiN + 2.2 μm TiCN) deposited on plasma nitrided PH15-5 steel enhanced the wear resistance. In fact, it is well known that the increase of the film thickness cannot only help to prolong the wear life but also seriously influence the adhesion between the film and the substrate. A possible solution to this problem is forming the graded structure and composition of the multilayer film due to their gradual properties in thermal expansion coefficient and lattice parameter. Therefore, this paper presented a 23.5 μm-thick TiN/TiCN multilayer film grown in graded structure by direct current magnetron sputtering (DCMS) technique, and the composition, microstructure, mechanical properties and wear resistance of the film were investigated.

2. Experimental section

The n-type Si (100) and 2520-310S steel wafers with 0.02 μm surface roughness were used as the substrates. TiN/TiCN multilayer film was prepared using DCMS system (SKY Technology Development Co., Ltd, JS-650) to sputter a planar rectangular titanium target (purity >99.5 wt.%, area 280 × 80 mm) in Ar (99.99%), N_2 (99.99%) and CH_4 (99.99%) mixed atmosphere. Before putting into the sputtering chamber, all of the substrates were ultrasonically cleaned in acetone and ethanol, respectively. Prior to deposition, the chamber was pumped down to a base pressure below 7×10^{-4} Pa. Thereafter, the substrates were cleaned by Ar^+ bombardments for 10 min at a pressure of 1.7 Pa with a pulsed substrate bias voltage of −1100 V, to remove thin oxide layer and other adherent impurities on the substrates. Then deposition was conducted at a bias voltage of −100 V (or a substrate ion current density of 2 mA/cm^2), a target current of 4 A and a distance from the substrate to the target of 100 mm. During deposition the substrate temperature increased from around 40 °C to 100 °C, and the total pressure of sputtering gas was controlled in a range of 0.4–0.5 Pa by the change of CH_4 flow rate. Before deposition of the TiN/TiCN multilayer film, a Ti buffer layer, which could be beneficial to good adhesion force [9], was deposited with about 1 μm. In order to obtain the TiN/TiCN multilayer film, the CH_4 flow rates were varied with the different deposition time as listed in Table 1.

The chemical composition of the film was analyzed by XPS (PHI-5702) with monochromated Al Kα radiation at a pass energy of 29.4 eV. The film was pre-etched for 2 min with Ar in order to remove the contaminations and oxidation layer on the film surface. Crystalline structure of the film was investigated by XRD using the Philips X'perts diffractometer (CuK_α line λ = 0.154 nm) at an incidence angle ranged from 1° to 90°.

* Corresponding author. Tel.: +86 931 4968236.
E-mail address: jyhao@licp.cas.cn (J. Hao).

0257-8972/$ – see front matter © 2012 Elsevier B.V. All rights reserved.
http://dx.doi.org/10.1016/j.surfcoat.2012.08.045

Table 1
The TiN/TiCN multilayer film obtained by variation of N_2 and CH_4 flow rates.

Ar flow rate (sccm)	N_2 flow rate (sccm)	CH_4 flow rate (sccm)	Work time (min)	Phase	Bilayer numbers
20	0→6	0	6	Ti→TiN	
20	6	0	2	TiN	
20	6	0→10	1.5	TiN→TiCN	
20	6	10	3	TiCN	1
20	6	10→0	1.5	TiCN→TiN	
20	6	0	2	TiN	
20	6	0→10	1.5	TiN→TiCN	
20	6	10	3	TiCN	2
–	–	–	–	–	–
20	6	10→0	1.5	TiCN→TiN	
20	6	0	6	TiN	
20	6	0→10	1.5	TiN→TiCN	
20	6	10	18.5	TiCN	30

The fractured cross-section of the multilayer film was confirmed by FESEM (JSM-6701F). Aiming to further determine the microstructure of the film, cross-sectional HRTEM (Tecnai G2 F20 S-Twin) with an acceleration voltage of 200 kV was applied.

The adhesion force of the total film was determined by scratch tester (Kaihua MFT-4000) with a conical diamond tip of 0.2 mm radius and 120° taper angle. Stanishevsky and Lappalainen [5] considered at least two staged in the film deformation and failure with the corresponding critical loads L_1 and L_2. L_1 was defined as the load at the first surface crack, and L_2 was named as the load at the whole film delaminated off the substrate. To investigate the morphology and depth of the scratch track, three dimension (3D) surface profilometry (Micro-XAM) was used. The hardness and elastic modulus were performed by using a nanoindenter (Nanotest 600) with a Berkovich diamond tip. The mean value of the hardness and elastic modulus of the film was obtained from the loading–unloading curves up to 5 times.

Wear tests were performed with a ball-on-disk reciprocating in UMT-2MT tribometer (Center for Tribology, Inc., CA, USA) at room temperature of about 20±5 °C and relative humidity of 40±5%. The AISI52100 steel balls were used as the counterparts with a diameter of 3 mm, a surface roughness of 20 nm and a hardness value of 850 HV. A sliding speed was 600 rpm, a load 4.0 N and a sliding stroke 5 mm. The feature of wear track in the TiN/TiCN multilayer film was surveyed by scanning electron microscope (SEM) (JSM-5600LV) with a resolution of 3.5 nm. 3D surface profilometry was employed to measure the depth and width of the wear track and calculate the wear rate. The composition of the transfer layer was determined by energy dispersive X-ray (EDX) spectroscopy.

3. Results and discussion

3.1. Composition and microstructure

XPS was used to determine the composition of the uppermost TiCN layer for the thick TiN/TiCN multilayer film. It was found that the uppermost layer contain carbon, titanium and nitrogen. In addition, Fig. 1 presents the XPS spectra of C 1s and N 1s of the uppermost layer. In the C 1s spectrum (Fig. 1a), three peaks were found at 282.0, 284.5 and 285.3 eV ascribed to C–Ti [10], C-sp^2 and C-sp^3 [11,12] bonds, respectively. This result shows that there is amorphous carbon (a-C) phase in the film. The N 1s spectrum (Fig. 1b) showed a characteristic band at 396.8 eV, which corresponded to the N–Ti bonds.

The XRD patterns of TiN/TiCN multilayer film obtained by using different incidence angles are shown in Fig. 2. All peaks corresponding to the (111), (200), (220), (311) and (222) plane of the cubic TiCN phase and TiN (111) phase were observed in the multilayer film. When the incidence angle was 1°, XRD pattern only reflected the information of the phase structure of the uppermost TiCN layer. However, the phase constituents of the multilayer film varied with the increase

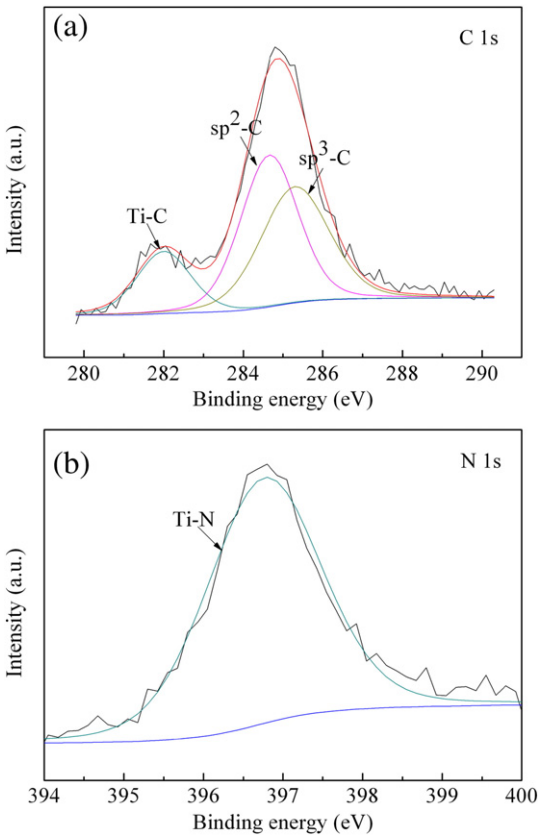

Fig. 1. XPS spectra of C 1s and N 1s of the uppermost TiCN layer.

of incidence angles due to the increase of the penetration depth of X-ray. As seen in Fig. 2, with the increase of incidence angle, the TiCN layers exhibited a transformation of preferred orientation from (220) to (111). It was explained that there was a different preferred orientation between the uppermost TiCN layer and the inner TiCN layers. The inner TiCN layers owned the greater stress than the uppermost TiCN layer, which resulted in the variation of preferred orientation [13]. Lim et al. [14] have also pointed that a high stress was produced in TiN film, where the (111) orientation was preferred. Moreover, with the increase of incidence angle, the XRD pattern gradually showed a TiN (111) peak, and that other TiN peaks were difficult to be observed due to their weak signals. In other words, the TiN layers also had a (111)

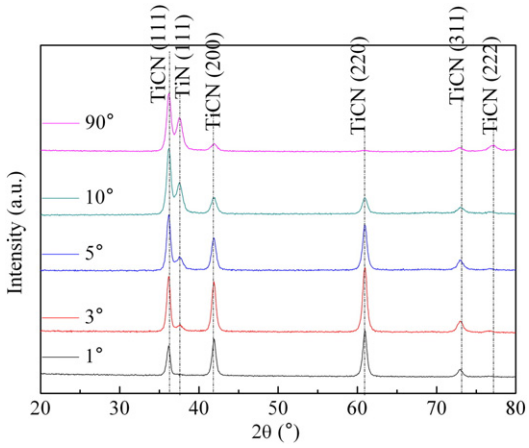

Fig. 2. XRD patterns of the TiN/TiCN multilayer film by using different incidence angles.

preferred orientation. This is an important phenomenon, and it suggests the distinct periodic structure in the TiN/TiCN multilayer film [15]. Meanwhile, it implies that the film structure is dense since the plane (111) orientation is the densely packed plane [16]. Other researchers [17] reported that the (111) preferred orientation and the shear stress of the slip system of TiN could lead to the high hardness of the film. In addition, it could be found that the peak intensity of the TiCN phase became weak except (111) orientation when the incidence angle increased. Under 10° and 90° of incidence angle, two similar XRD patterns meant that the phase constituents hardly changed.

The grain size of TiCN and TiN layer was determined with preferred orientation in Bragg plane by using the Sherrer equation [18] as given in Fig. 3. Nevertheless, Strauss et al. [19] have not considered the effect of the strain on the broadening of XRD peak when calculating the grain size by the above method. Therefore, the grain size calculated herein was approximate. The grain size of TiCN and TiN layer decreased firstly and then stabilized with the increase of incidence angle. According to the information in Fig. 2, it could be conjectured that the grain size of the uppermost TiCN layer was about 16.3 nm in (220) plane with 1° of incidence angle and the average gain size of the TiCN layers was 11.4 nm in (111) plane with 90° of incidence angle. This may be attributed to the transformation of preferred orientation from the uppermost TiCN layer to the inner TiCN layer. Besides, the average grain size of the TiN layers was about 9.0 nm measured in (111) plane with 90° of incidence angle. It must be pointed out that when the incidence angle was 90°, the values of the full width at half maximum (FWHM) of (111) peaks of TiCN layer and TiN layer were about 0.72 and 0.92, respectively, obtained by using Cauchy–Gauss sum functions in the fitting procedure. From above, it can be deduced that the thick TiN/TiCN multilayer film contains nanometer-sized (10–20 nm) crystals of TiCN and TiN [20] and a-C phase.

The FESEM micrograph and HRTEM image of the film are shown in Fig. 4. As described in Fig. 4(a), the thickness of the whole film was about equal to 23.5 μm. Then the dark TiCN layer and light TiN layer allowed a clear determination of the layered structure in Fig. 4(c). It was found that the TiN layer shows the distinct columnar structure. The thickness of the bilayer (namely, the modulation period) was about 0.81 μm including around 0.57 μm TiCN layer and 0.24 μm TiN layer, when the bilayer numbers ranged from 2 to 29. In view of the layer thickness and the deposition time of each layer, the deposition rates of TiN layer and TiCN layer are about 0.07 μm/min and 0.13 μm/min. It is worth pointing out that the deposition rates are approximate value since the deposition time of TiN layer and TiCN layer is 3.5 min and 4.5 min, respectively, through dividing the grading time equally between them.

It could be observed from Fig. 4(a) and (b) that the uppermost TiCN layer displayed a columnar structure, while the inner TiCN layers presented a featureless structure. Thus, in order to further illustrate

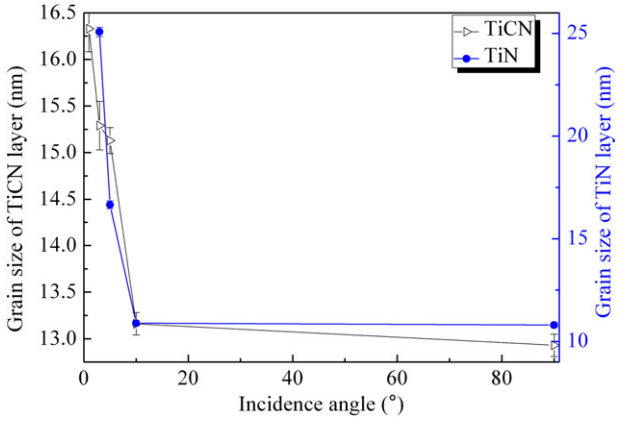

Fig. 3. Grain size of TiCN and TiN layer as a function of incidence angle.

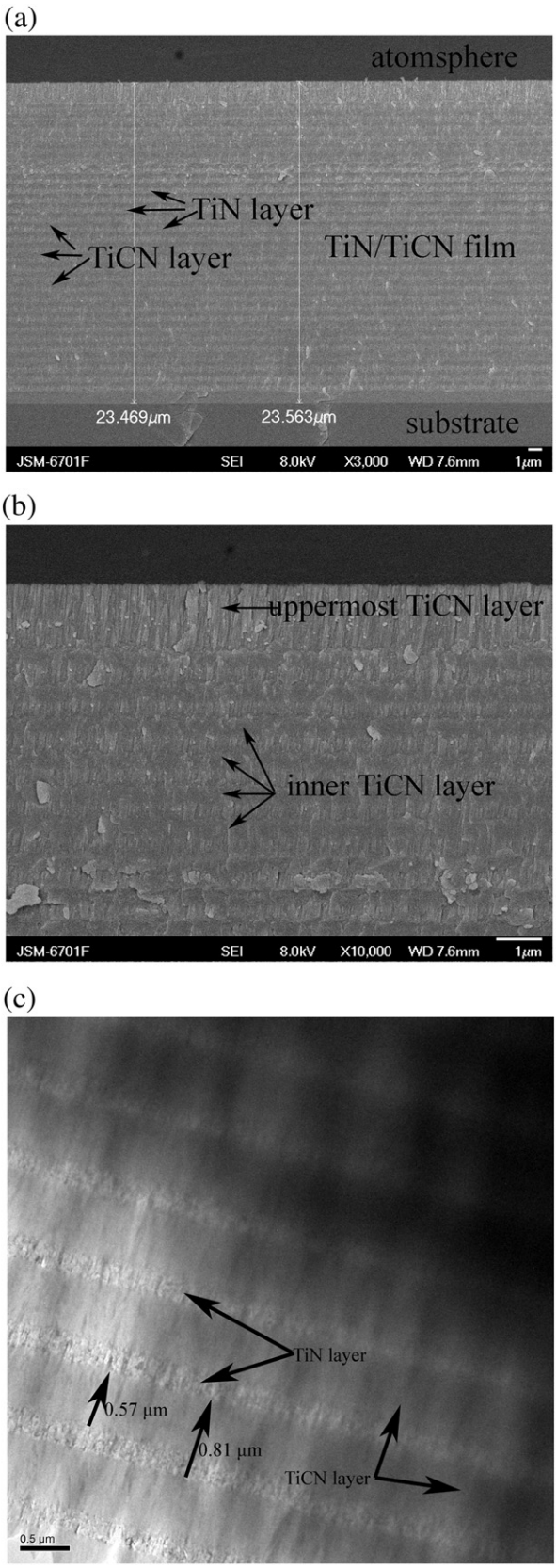

Fig. 4. Fractured cross-section of the TiN/TiCN multilayer film: (a) FESEM micrograph of the whole film, (b) magnified FESEM image of the film top, and (c) HRTEM image of the segment film.

the difference of the microstructure between the uppermost TiCN layer and the inner TiCN layer, their HRTEM enlargement images and corresponding selected area electron diffraction (SAED) patterns are shown in Figs. 5 and 6, respectively. It could be observed in Fig. 5(a) that there were many columnar crystals in the uppermost TiCN layer. When measuring the lattice constant of the periodic arrangement (0.22 nm) was greater than half the value of the TiCN lattice constant (0.215 nm), the supersaturated solid solution could be formed in the uppermost TiCN layer. However, as seen in Fig. 5(b), the uppermost TiCN layer only presented a small number of a-C. This result was some deviation on the XPS data, which showed that the C relative contents reached around 50 at% measured by XPS and a small fraction of C atoms were bonded to Ti atoms in Fig. 1a. It can be conjectured that the excess a-C dissolved in the TiCN lattice leads to forming the supersaturated solid solution. The reason of the formation of the supersaturated solid solution has been elaborated in detail by our previous work [21]. Therefore, the uppermost TiCN layer showed a columnar structure. The amorphous mixing region embedded with some nanocrystallites, which agrees with the other researcher [22,23], was found in Fig. 6. This result is in accordance with the FESEM image. In addition, the diffraction patterns revealed that the crystal structures of two kinds of TiCN layers were different. The uppermost TiCN layer showed a slight (220) preferred orientation, whereas in the inner

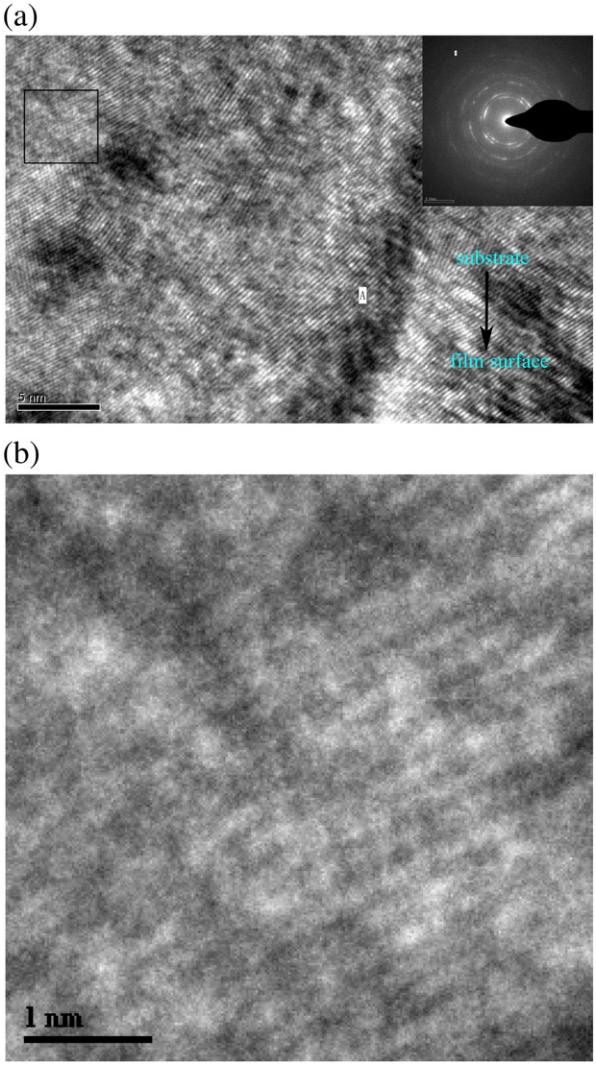

Fig. 5. The uppermost TiCN layer: (a) HRTEM image [The upper inset shows the corresponding diffraction pattern.], (b) magnified section with selection rectangle from (a).

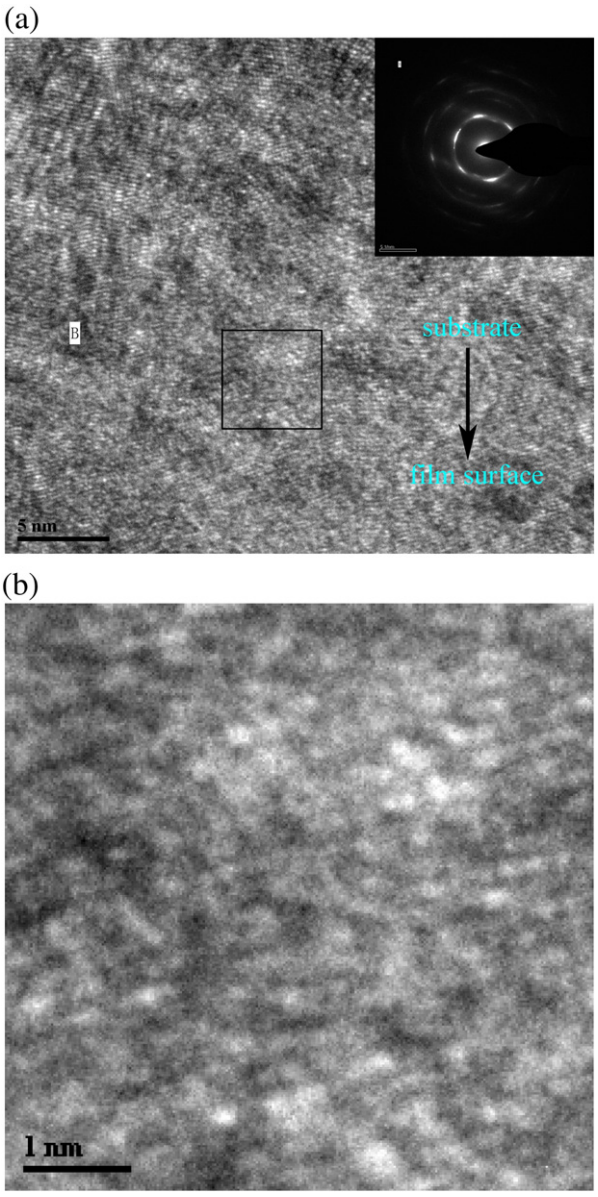

Fig. 6. The inner TiCN layer: (a) HRTEM image [The upper inset shows the corresponding diffraction pattern.], (b) magnified section with selection rectangle from (a).

TiCN layer, there was preferred orientation of the (111) plane. This result is consistent with the XRD results.

As mentioned above, all the inner TiCN layers possess a nanocomposite structure including the TiCN nanocrystalline and the a-C, and the TiN layers only reveal the TiN nanocrystalline. These multi- and single-phase structure will certainly affect the mechanical and tribological properties of the film.

3.2. Mechanical properties

The critical loads of the film prepared on the steel substrate were hardly determined by the acoustic emission (AE) signal and friction force during scratch test due to a legible layered structure and the different friction coefficient values between the TiN layer and the TiCN layer. The layered structure was easy to cause the noise when the failure occurred in the interface of TiN and TiCN layer. Therefore, the critical loads only were calculated by the distance from zero to failing point multiplied by the total load (defined as a value of the load from initial running to stop) and then divided by the total distance. Fig. 7 describes the 2D micrograph of scratch track of the film. It could be found that the

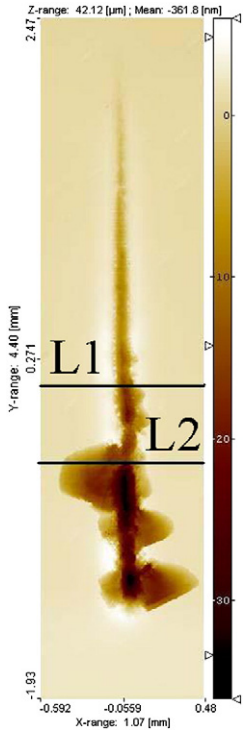

Fig. 7. The 2D micrograph of the scratch track of the TiN/TiCN multilayer film.

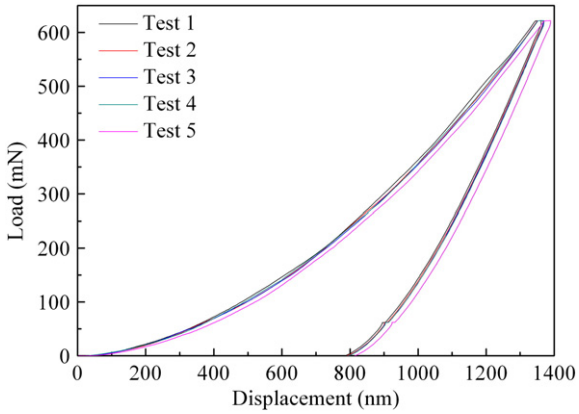

Fig. 8. Nano-indentation load–displacement curves for the TiN/TiCN multilayer film.

failures propagated along the vertical direction of scratching direction, causing flaking of the film inside and at the edges of the scratch track. From Figs. 4 and 5, it could be concluded that the film failed by flaking rather than by cracking or delaminating due to the long needle-like columnar crystals existing in the film [24]. Based on the above information, the values of L_1 and L_2 were 23.5 and 29.0 N, respectively. In addition, the depths of L_1 and L_2 measured by 3D surface profilometry were about 18.0 and 22.5 μm, which mean that the film was incomplete failure in L_1. Accordingly, the value of the L_2 (29.0 N) reflected the real adhesion force between the film and the steel substrate. In comparison with the results of other authors [5,25], the film presented a normal adhesion force as the thickness of the film achieved 23.5 μm. There are some reasons to clarify this result. Firstly, the film provides a gradual change of the composition either from the Ti buffer layer to TiN layer or from the TiN layer to TiCN layer. This is helpful in reducing the interfacial stress as well as maintaining the adhesion force as increasing the thickness [26]. Then, the appropriate thickness TiN layer in the multilayer film can improve the adhesion force [27]. In fact, the thickness ratio of TiN layer and TiN/TiCN bilayer has been discussed in our previous experiments. When the ratio is approximately 30%, the TiN/TiCN multilayer films possess good mechanical and tribological properties, in agreement with the result of other researchers [28]. Finally, the adhesion force can also be ascribed to the ability of TiCN nanocrystalline and a-C in the TiCN layer to distribute the applied stress over a broad area as proposed by others [29,30].

Fig. 8 shows the load–unload curves of TiN/TiCN multilayer film with maximum indentation depth being kept at around 1.39 μm. The mean values of hardness and elastic modulus of the film deposited on steel substrate were about 21.4 GPa and 297.9 GPa, respectively. It has been reported that the hardness of TiN, TiCN and TiN/TiCN films (0.5–6 μm) is in the range from 8.2 GPa to 17.0 GPa [9,31], 18.8 GPa to 22.2 GPa [32,6] and 20.4 GPa to 27.3 GPa [33,34], respectively. In addition, the hardness of thin TiCN and TiN/TiCN films (about 2.0 μm and 9.9 μm), which was 32.0 GPa and 27.2 GPa, was also obtained in our previous work. However, it was well known that both the excessive thickness (>10 μm) and high modulation period seriously influenced the mechanical properties of the film [15,35,36]. Thus, the hardness value of the film was satisfactory with the film thickness of 23.5 μm. The fact that the hardness is maintained in normal level even if in high film thickness can be explained that dislocation movement is suppressed by the small grains and the narrow space between the nanocrystalline particles, like the space between TiCN particles less than 0.22 nm as shown in Figs. 5(a) and 6(a) [37]. On the other hand, the mixed structure of nanocrystalline and amorphous phase in the TiCN layer can increase the cohesive energy of the interface boundaries, which effectively restrains the grain boundary slip and enhances the film hardness [38]. Besides, the elastic recovery parameter (R) of the film was calculated by using the following equation [39,40]:

$$R = \frac{\delta_{\max} - \delta_p}{\delta_{\max}} \times 100\% \quad (1)$$

where $\delta_{\max}$ and δ_p are the maximum and residual of plastic displacement, respectively. According to the equation and the data listed in Fig. 8, the mean value of the elastic recovery parameter was about 42.2%. Furthermore, it is generally known that the ability of a film to resist mechanical degradation and failure is improved by a high H/E or H^3/E^2 [22,41]. In view of the condition, the values of H/E and H^3/E^2 for the film were 0.072 and 0.11 GPa, respectively. The low value of R and H/E can imply a weak resistance to crack for the film, which has been shown in the above section [42]. However, the TiN/TiCN multilayer film has a good resistance to plastic deformation due to $H^3/E^2 > 0.1$ [43]. For the tribological films, the H^3/E^2 ratio as a key parameter always predicts the tribological behavior [25]. The details will be discussed below.

3.3. Tribological properties

The friction coefficient of the film deposited on steel substrate was measured against steel balls. Fig. 9 shows the friction curve of TiN/TiCN multilayer film. Accordingly, the wear track of the film is displayed in Fig. 10. As seen in Fig. 9, it could be observed that the friction coefficient of film presented remarkable stage characteristics. It started with around 0.46 and after 0.25 h reduced to around 0.16. When the sliding time reached 2.5 h, the friction coefficient rose to about 0.26 and had certain fluctuation. Later on, the friction coefficient was alternately high and low. With respect of the change of the friction coefficient, the composition of transfer layer and friction interface should be taken into account [44]. Firstly, the high friction coefficient occurs in running period due to lack of transfer layer. Then, possibly forming the a-C transfer layer reduces the friction coefficient. As XPS results and HRTEM images were mentioned above, it showed that the a-C existed in the TiCN layers deposited by DCMS. Due to the low shear strength, a-C is known to exhibit low friction coefficient and can be used as a solid lubricant. In addition, the common tenor in the literature concerning the tribology of carbon-based coatings links the low-friction behavior to the formation

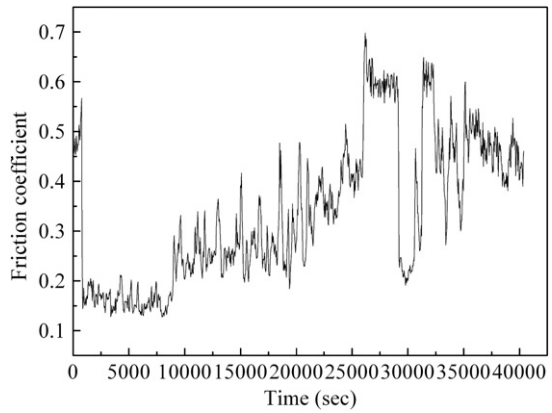

Fig. 9. The friction curve of the TiN/TiCN multilayer film.

of 3rd bodies in the contact and the subsequent formation of lubricious transfer layer [45]. Therefore, the low friction coefficient could be considered an action of a-C transfer layer. Following it, the increase and fluctuation of the friction coefficient can be attributed to a combination of a-C transfer layer and friction interface between TiN layer and steel balls [46]. Finally, under high load, long sliding time and high friction coefficient, the tribochemical reactions occur in the friction interface. As seen in Fig. 10(b), the composition of the transfer layer in Fig. 10(a) contained the titanium (Ti), carbon (C), nitrogen (N), oxygen (O) and iron (Fe). Among them, Fe atoms derived from the steel ball reacts with the oxygen (O_2) and produces the iron oxide, which results in the increase of friction coefficient. In addition, when the friction is implemented in the interface of TiN layer and steel ball, there is a high friction coefficient in the film. On the contrary, the film has a good friction behavior. This is the main reason for the steep climbs and descents of the friction coefficient.

As mentioned with H^3/E^2, it is predicted that the film has a good wear resistance. In fact, the wear rate of the film was 1.59×10^{-6} mm^3/N m sliding over 11 h. Then the depth of the wear track was about 12.0 μm in Fig. 10(c), which implied that the service life of the film could exceed 20 h at the same condition. In a word, compared with the wear rate of the single layer films (TiCN, TiN) and the thin hard films [19,47,48], the wear rate of the thick TiN/TiCN multilayer film basically remains stable, however, its service life has a prominent improvement.

4. Conclusions

The thick TiN/TiCN multilayer film, of which the thickness was 23.5 μm, was deposited on steel and Si substrates by DCMS. The uppermost TiCN layer and the inner TiCN layers of the film had the different preferred orientation determined by XRD. Moreover, the inner TiCN layers possessed nanocomposite structure consisting of the TiCN nanocrystalline and the amorphous carbon, and the TiN layers showed nano-columnar structure. By the scratch tests and nano-indentation, the film showed an appreciable adhesion force and a satisfactory hardness even if the thickness is 23.5 μm. Tribological test results also indicated that there was no significant change in the wear resistance of the film in contrast with other thin hard films, but the service life of the film was prolonged by the high thickness.

Acknowledgments

The authors are grateful to the National Nature Science Foundation of China (50905177) for financial support.

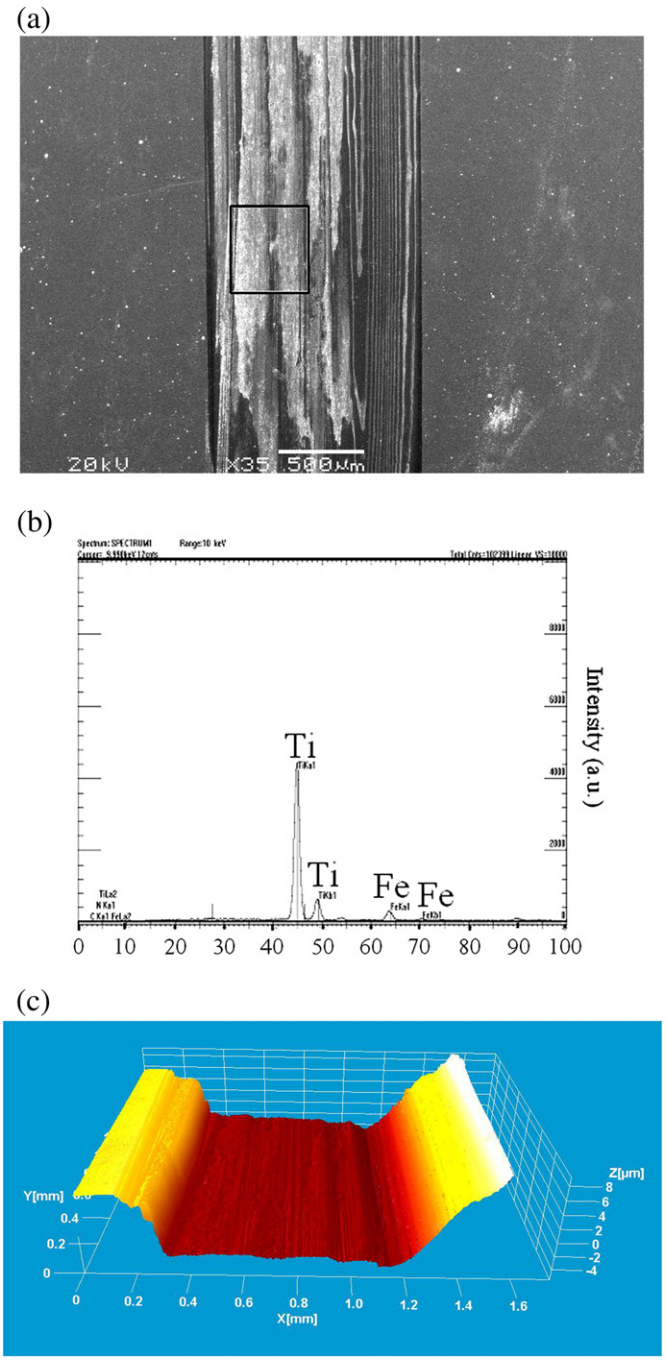

Fig. 10. The wear track of the TiN/TiCN multilayer film: (a) SEM micrograph, (b) EDX analysis corresponding to the composition of black box in (a), (c) 3D image.

References

[1] Y.L. Shi, H.R. Peng, Y. Xie, G.W. Xie, C. Zhao, S.Z. Li, Surf. Coat. Technol. 132 (2000) 26.
[2] I. Endler, M. Hohn, M. Herrmann, H. Holzschuh, R. Pitonak, S. Ruppi, H. van den Berg, H. Westphal, L. Wilde, Surf. Coat. Technol. 205 (2010) 1307.
[3] B.A. Behrens, A. Huskic, Materialwiss. Werkst. 36 (2005) 218.
[4] L.C. Agudelo, R. Ospina, H.A. Castillo, A. Devia, Phys. Scr. T131 (2008) 014006.
[5] A. Stanishevsky, R. Lappalainen, Surf. Coat. Technol. 123 (2000) 101.
[6] J.P. Tu, R. Chen, D.G. Liu, Y.J. Mai, C.D. Gu, Surf. Coat. Technol. 205 (2011) 5228.
[7] Y.L. Su, W.H. Kao, J. Mater. Eng. Perform. 7 (1998) 601.
[8] A. Raveh, I. Zukerman, H. Kalman, J.E. Klemberg-Sapieha, L. Martinu, Wear 263 (2007) 1249.
[9] G.S. Kim, S.Y. Lee, J.H. Hahn, B.Y. Lee, J.G. Han, J.H. Lee, S.Y. Lee, Surf. Coat. Technol. 171 (2003) 83.

[10] N.K. Manninen, R.E. Galindo, N. Benito, N.M. Figueiredo, A. Cavaleiro, C. Palacio, S. Carvalho, J. Phys. D Appl. Phys. 44 (2011) 75501.
[11] D.V. Shtansky, K.A. Kuptsov, P.V. Kiryukhantsev-Korneev, A.N. Sheveiko, A. Fernandez, M.I. Petrzhik, Surf. Coat. Technol. 205 (2011) 4640.
[12] Z.W. Xie, L.P. Wang, X.F. Wang, L. Huang, Y. Lu, J.C. Yan, Appl. Surf. Sci. 258 (2011) 1206.
[13] W.J. Chou, G.P. Yu, J.H. Huang, Surf. Coat. Technol. 149 (2002) 7.
[14] S.H.N. Lim, D.G. McCulloch, S. Russo, M.M.M. Bilek, D.R. McKenzie, Nucl. Instrum. Meth. Phys. Res. B 190 (2002) 723.
[15] M. Balaceanu, M. Braic, V. Braic, G. Pavelescu, Surf. Coat. Technol. 200 (2005) 1084.
[16] R.A. Antunes, A.C.D. Rodas, N.B. Lima, O.Z. Higa, I. Costa, Surf. Coat. Technol. 205 (2010) 2074.
[17] C.T. Chen, Y.C. Song, G.P. Yu, J.H. Huang, J. Mater. Eng. Perform. 7 (1998) 324.
[18] H.P. Klug, L.E. Alexander, X-ray Diffraction Procedures: For Polycrystalline and Amorphous Materials, second ed. Wiley-Interscience, New York, 1974.
[19] H.W. Strauss, R.R. Chromik, S. Hassani, J.E. Klemberg-Sapieha, Wear 272 (2011) 133.
[20] R. Hauert, J. Patscheider, L. Knoblauch, M. Diserens, Adv. Mater. 11 (1999) 175.
[21] J. Zheng, J. Hao, X. Liu, W. Liu, J. Phys. D Appl. Phys. 45 (2012) 095303.
[22] J.L. Lin, J.J. Moore, B. Mishra, M. Pinkas, W.D. Sproul, Acta Mater. 58 (2010) 1554.
[23] J.C.F. Rodríguez-Reyes, C. Ni, H.P. Bui, T.P. Beebe, A.V. Teplyakov, Chem. Mater. 21 (2009) 5163.
[24] Z. Qi, P. Sun, Z. Wang, in: J. Luo, Y. Meng, T. Shao, Q. Zhao (Eds.), Microstructure and Mechanical Properties of TiCN Coatings Prepared by MTCVD, Springer, Berlin Heidelberg, 2010, p. 796.
[25] S. Guruvenket, D. Li, J.E. Klemberg-Sapieha, L. Martinu, J. Szpunar, Surf. Coat. Technol. 203 (2009) 2905.
[26] P. Jedrzejowski, J.E. Klemberg-Sapieha, L. Martinu, Thin Solid Films 466 (2004) 189.
[27] S.J. Bull, D.G. Bhat, M.H. Staia, Surf. Coat. Technol. 163 (2003) 507.
[28] I. Zukerman, A. Raveh, Y. Landau, R. Weiss, R. Shneck, Y. Shneor, H. Kalman, J. Klembergsaphieha, L. Martinu, Surf. Coat. Technol. 201 (2007) 6171.
[29] K. Holmberg, A. Matthews, H. Ronkainen, Tribol. Int. 31 (1998) 107.
[30] S. Veprek, A.S. Argon, Surf. Coat. Technol. 146 (2001) 175.
[31] A.M. Peters, M. Nastasi, Vacuum 67 (2002) 169.
[32] T. Sangkla, S. Bland, K. Tuchinda, in: S.I. Ao, L. Gelman, D.W. Hukins, A. Hunter, A.M. Korsunsky (Eds.), Proceedings of the World Congress on Engineering, IAENG, London, 2011, WCE 2011.
[33] E. Bemporad, C. Peechio, S. De Rossi, E. Carassiti, Surf. Coat. Technol. 146 (2001) 363.
[34] M.D. Bao, X.B. Xu, H.J. Zhang, X.P. Liu, L.H. Tian, Z.X. Zeng, Y.B. Song, Thin Solid Films 520 (2011) 833.
[35] S.K. Tien, J.G. Duh, Thin Solid Films 494 (2006) 173.
[36] Y.L. Yang, D. Zhang, W. Yan, Y.R. Zheng, Opt. Lasers Eng. 48 (2010) 119.
[37] S. Veprek, Thin Solid Films 317 (1998) 449.
[38] S. Hassani, J.E. Klemberg-Sapieha, L. Martinu, Surf. Coat. Technol. 205 (2010) 1426.
[39] V. Hajek, K. Rusnak, J. Vlcek, L. Martinu, H.M. Hawthorne, Wear 213 (1997) 80.
[40] C. Morant, P. Prieto, A. Forn, J.A. Picas, E. Elizalde, J.M. Sanz, Surf. Coat. Technol. 180–181 (2004) 512.
[41] J.E. Klemberg-Sapieha, P. Jedrzejowski, L. Martinu, J. Superhard. Mater. 29 (2007) 147.
[42] J. Musil, J. Sklenka, R. Cerstvy, Surf. Coat. Technol. 206 (2012) 2105.
[43] J. Musil, R. Jilek, M. Meissner, T. Tolg, R. Cerstvy, Surf. Coat. Technol. 206 (2012) 4230.
[44] Y.H. Cheng, T. Browne, B. Heckerman, E.I. Meletis, Surf. Coat. Technol. 205 (2011) 4024.
[45] M.R. de Figueiredo, J. Neidhardt, R. Kaindl, A. Reiter, R. Tessadri, C. Mitterer, Wear 265 (2008) 525.
[46] M. Mahdipoor, F. Mahboubi, S. Ahangarani, M. Raoufi, H. Elmkhah, J. Mater. Eng. Perform. 20 (2011) 1.
[47] J.C. Sánchez-López, M.D. Abad, I. Carvalho, R. Escobar Galindo, N. Benito, S. Ribeiro, M. Henriques, A. Cavaleiro, S. Carvalho, Surf. Coat. Technol. 206 (2012) 2192.
[48] F. Zhou, Q.Z. Wang, X.N. Wang, K.M. Chen, M.L. Wang, T. Qian, Y.X. Li, Appl. Surf. Sci. 257 (2011) 7813.